

Detection of crossing white matter fibers with high-order tensors and rank- k decompositions

Fangxiang Jiao*, Yaniv Gur*, Chris R. Johnson and Sarang Joshi

SCI Institute, University of Utah, Salt Lake City, UT 84112, USA
{fjiao, yanivg, crj, sjoshi}@sci.utah.edu

Abstract. Fundamental to high angular resolution diffusion imaging (HARDI), is the estimation of a positive-semidefinite orientation distribution function (ODF) and extracting the diffusion properties (e.g., fiber directions). In this work we show that these two goals can be achieved efficiently by using homogeneous polynomials to represent the ODF in the spherical deconvolution approach, as was proposed in the Cartesian Tensor-ODF (CT-ODF) formulation. Based on this formulation we first suggest an estimation method for positive-semidefinite ODF by solving a linear programming problem that does not require special parametrization of the ODF. We also propose a rank- k tensor decomposition, known as CP decomposition, to extract the fibers information from the estimated ODF. We show that this decomposition is superior to the fiber direction estimation via ODF maxima detection as it enables one to reach the full fiber separation resolution of the estimation technique. We assess the accuracy of this new framework by applying it to synthetic and experimentally obtained HARDI data.

1 Introduction

The imaging technique known as Diffusion Tensor MRI (DT-MRI) measures the Brownian motion of water molecules in a tissue and enables one to reveal its diffusion properties. It is primarily used to infer the white matter connectivity of the brain. The signal attenuation model in DT-MRI is given by the Stejskal-Tanner equation

$$S(\mathbf{g}) = S_0 \exp(-bD(\mathbf{g})), \quad (1)$$

where $D(\mathbf{g})$ is the apparent diffusion coefficient (ADC) in the direction \mathbf{g} . In traditional DTI the ADC is modeled by a quadratic form $\mathbf{g}^T \mathbf{D} \mathbf{g}$, where \mathbf{D} is a second-order tensor known as diffusion tensor. Since $D(\mathbf{g})$ is a quadratic form, the modeled ADC is elliptic and thus cannot model complex structures such as crossing fibers. To overcome the limitations of DTI, High Angular Resolution Diffusion Imaging (HARDI) is used. Different modalities and estimation techniques associated with HARDI have been proposed over the years. These methods include the multi-compartment model [25], Q-ball imaging (QBI) [24, 10], spherical deconvolution [22, 2], Diffusion Orientation Transform (DOT) [17],

* These authors contributed equally to this work.

OPDF [23] and methods that describe the ADC profile using high-order tensors [4, 6]. These latter methods represent $D(\mathbf{g})$ as an even-order homogeneous polynomial whose coefficients are identified with the entries of a high-order tensor. The resulting function can describe multiple maxima and can be used to model complex fiber structures. Unfortunately, in contrast to the diffusion tensor model, the maxima of the ADC profile described by a high-order homogeneous polynomial, do not correspond to the underlying fiber directions. This is solved by computing the diffusion propagator and locating the fiber directions at its local maxima. This computation involves a non-trivial Fourier transform step that adds complexity to the estimation process. To solve this problem, it was proposed in [26] to combine the high-order tensor formulation with the spherical deconvolution technique. This strategy enables one to estimate a positive-definite ODF, dubbed Cartesian Tensor-ODF (CT-ODF), whose maxima correspond to the orientations of the fibers.

Although finding all the local maxima's of high order spherical functions is not trivial, only a handful of papers have been devoted to this important issue [7, 1, 19]. It turns out that since each maximum has a finite width, maxima tend to interfere below a certain fiber separation angle. Therefore, using maxima finding, the maximal fiber separation resolution enabled by the data acquisition technique cannot be reached. An interesting solution to this problem was proposed in [19]. The ODFs in that case were estimated using the Q-Ball imaging technique and then were converted to high-order tensors using a linear transformation. Then, a heuristic rank- k tensor approximation was applied to the tensors to extract the fiber directions beyond the resolution limit determined by the maxima. This method was later used to initialize the ball-and-stick model [20]. Although the proposed method was applied successfully to synthetic and real data, it has some inherent limitations: To calculate the different rank-1 tensors that contribute to the rank- k approximation, rank-1 tensor subtractions were used. It is known that rank-1 tensor subtractions can potentially increase the tensor rank [21] and hence the convergence of the algorithm is not guaranteed. Furthermore, although the initial ODF is non-negative, the residuals obtained by these subtractions do not have this property. In this paper we address these problems and in addition to a new ODF estimation technique, we propose an alternative way to decompose the tensors.

The paper is organized as follows: We first develop the estimation technique for positive-semidefinite ODFs of any order. This estimation method is based on the CT-ODF formulation for high-order tensors proposed by Angelos et. al. [26]. Then, we formulate the estimation problem as a linear programming problem with linear constraints that enforce non-negativity of the ODF. For extracting the individual fiber properties we apply a rank- k tensor decomposition, known as the CP decomposition, to the ODF. In addition to providing the fiber directions, the decomposition also enables us to estimate the fiber fractions. Finally, we demonstrate our proposed technique on synthetic and real HARDI data and show that the proposed algorithm provides accurate results and can reliably resolve two crossing fibers with much higher fidelity than by maxima detection.

We confirm the accuracy of the algorithm on both synthetic, phantom and real HARDI data.

2 Spherical deconvolution

Following the work by Tournier et al. [22], the Diffusion-Weighted MR signal can be modeled by a spherical convolution of an orientation distribution function (ODF) with an axially symmetric kernel, K :

$$S(\mathbf{g}, b) = S_0 \int_{S^2} F(\mathbf{v}) K(\mathbf{g}, \mathbf{v}, b) d\mathbf{v}, \quad (2)$$

where \mathbf{g} is the gradient direction. The function F is associated with the ODF (or fiber-ODF in Tournier’s original work), and it is composed of a sum of k delta functions, each is oriented along one fiber direction and weighted according to the corresponding fiber fraction. The kernel K can be chosen in various ways depending on the dataset and the region in the brain (e.g., [5, 2]). A very common choice is the single fiber response which is described by the bipolar Watson function

$$K(\mathbf{g} \cdot \mathbf{v}, b) = e^{-c(\mathbf{g}^T \mathbf{v})^2}, \quad (3)$$

where the concentration parameter, c , is a function of the b value and the diffusivity. Given the measured DW-signal and a kernel, which is known a priori, the ODF is computed by performing spherical deconvolution of K from $S(\mathbf{g}, b)$. Technically, this may be solved using least-squares where the solution is given by a simple pseudo-inverse operation [22].

In [26] it was proposed to represent F as a spherical, even-order and positive-definite homogeneous polynomial induced by a high-order tensor. In that work it was suggested to use the single fiber response kernel described in Eq. (3). The concentration parameter was chosen to be large enough to describe a diffusion process which is highly restricted perpendicular to the orientation \mathbf{v} . We use the same ideas here.

2.1 Estimation of positive-semidefinite ODF using spherical deconvolution

Any ODF estimated from the data has to be non-negative. In [26] a special parametrization was used to yield a positive-definite ODF. In this section we show that the same goal can be achieved by minimizing an objective function subject to linear constraints that enforce the positivity on the ODF. That is, given measurements in n gradient directions, we aim to solve the following problem:

$$\min_F \frac{1}{2} \sum_{i=1}^n \left\| S(\mathbf{g}_i, b) - S_0 \int_{S^2} F(\mathbf{v}) K(\mathbf{g}_i, \mathbf{v}, b) d\mathbf{v} \right\|^2 \quad (4)$$

subject to

$$F(\mathbf{g}_i) \geq 0, \quad \mathbf{g}_1, \dots, \mathbf{g}_n \in S^2.$$

The solution to this problem guarantees positive-semidefiniteness in the discrete sense, that is, in the directions which were used to acquire the signal. We believe that under certain conditions the estimated ODF will be positive-semidefinite in every direction on the sphere. However, since this is an open problem, we leave the complete mathematical study as future work.

We now formulate the problem explicitly. This formulation holds for tensors of any order, however, in this paper we only consider fourth-order tensors that are also *supersymmetric*. Here we will refer to a supersymmetric tensor by using the term *symmetric*. The coefficients of a symmetric fourth-order tensor are invariant under any permutation of the indices. Thus, a symmetric fourth-order tensor has 15 unique coefficients associated with a homogeneous polynomial:

$$F(\mathbf{g}) = \sum_{a=0}^4 \sum_{b=0}^{4-a} c_{ab} g_1^a g_2^b g_3^{4-a-b}, \quad (5)$$

where c_{ab} denote the unique tensor coefficients and g_1, g_2 and g_3 are the components of the gradient direction \mathbf{g} .

Substituting F into the integral (2), we have a sum of integrals, each related to a different monomial:

$$S(\mathbf{g}, b) = \sum_{a=0}^4 \sum_{b=0}^{4-a} c_{ab} \int_{\mathbf{v} \in S^2} v_1^a v_2^b v_3^{4-a-b} K(\mathbf{g}, \mathbf{v}, b) d\mathbf{v}. \quad (6)$$

Solving these integrals analytically is intractable, hence, we approximate each one of them according to the centroid rule for integration of functions on the sphere [3]. Given a sphere triangulation with N faces, for a spherical function, $f(\mathbf{v})$, the centroid rule is given by

$$\int_{S^2} f(\mathbf{v}) d\mathbf{v} \approx \sum_{i=1}^N f(\mathbf{v}_i) A(\Delta_i) \quad (7)$$

where \mathbf{v}_i is the centroid of the i 'th face and $A(\Delta_i)$ is the area of the face. This scheme is very accurate for specific sphere triangulations. Here we choose the third-order icosahedron triangulation which results in 1280 faces (642 nodes). The evaluation of each integral according to this scheme is very fast as the centroids and the areas of the faces are computed only once.

Following these calculations we can define a matrix, C , whose entries correspond to the numerical approximation of (7) for each monomial, in each direction \mathbf{g}_i . The size of this matrix is then $n \times m$ where n is the number of gradient directions and m is the number of unique tensor coefficients.

The linear constraints that impose the positivity on F are defined by using a $n \times m$ matrix A . Each row of A corresponds to a different gradient direction, and each column corresponds to a different monomial. The multiplication $A\mathbf{x}$ results in a n -dimensional vector, each element of it corresponds to $F(\mathbf{g}_i)$, where F is defined by Eq. (5). Thus, we obtain a set of n linear constraints, each constraint is applied to a different gradient direction.

Finally, with respect to the matrices defined above, for each voxel we solve the following linear programming problem:

$$\arg \min_{\mathbf{x}} \frac{1}{2} \|\mathbf{S} - \mathbf{C} \cdot \mathbf{x}\|^2 \quad \text{subject to} \quad -\mathbf{A}\mathbf{x} \leq \mathbf{b}, \quad (8)$$

where \mathbf{S} is a vector of the n DW measurements, and \mathbf{b} is a n -dimensional vector which defines the boundary of the convex polytope on which we minimize the objective function. Setting the values of \mathbf{b} to be zero results in estimation of a positive-semidefinite ODF.

To solve this problem, the number of gradient directions has to be larger than the number of the tensor coefficients. Since, typically, in HARDI scans $n > 60$, this condition holds as a fourth-order homogeneous polynomial defined by $m = 15$ unique coefficients. This problem may be solved efficiently using MatLab optimization toolbox or through open source packages for convex optimization such as CVX [11]. Given the optimal vector of coefficients, \mathbf{x}^* , the ODF is computed by $F = \mathbf{A}\mathbf{x}^*$. The unique tensor coefficients are then arranged in a fourth-order tensor using the symmetry and the appropriate monomial factors.

Once the ODF has been estimated we proceed to extracting the fiber directions and fractions. As an ODF is associated with a finite-order expansion of spherical harmonics, its maxima has a finite width. Thus, the ODF's maxima interfere and do not correspond to the correct fiber directions below a certain separation angle. In the following section we solve this problem by using a rank- k tensor decomposition known as the CP decomposition. We show that while a rank-1 decomposition corresponds to finding the maxima of F , a decomposition with $k > 1$ corresponds to finding the different components (fibers) that contribute to F which, in turn, significantly increases the ability to separate crossing fibers.

3 High-order tensor decompositions

To discuss HOT decompositions we have to first define the notion of a *tensor-rank*. Tensor rank, denoted here as $R = \text{rank}(\mathcal{D})$, is defined as the minimal number of terms such that the following equality holds

$$\mathcal{D} = \sum_{r=1}^R \mathbf{v}_r^1 \otimes \mathbf{v}_r^2 \otimes \dots \otimes \mathbf{v}_r^n, \quad (9)$$

where \mathbf{v} are first-order tensors (vectors). The *order* of the tensor, n , is defined by the number of its indices and it determines the number of tensor products in Eq. (9). A *cubic* tensor, is a tensor whose different modes have the same size, i.e., $\mathcal{D} \in \mathbb{R}^{d \times d \times \dots \times d}$. The decompositions that we discuss in this section hold for a general n 'th-order tensor which is not necessarily cubic or symmetric. In our case \mathcal{D} is cubic and symmetric where $n = 4$ and $d = 3$.

Unlike the matrix case ($n = 2$), the rank of a given HOT is not known. In fact, the problem of determining the rank of a given tensor is NP-complete [12].

However, in this work we are interested in low-rank tensor approximation. For a given tensor rank $k < R$, the low-rank approximation is defined by:

$$\mathcal{D} \approx \sum_{r=1}^k \lambda_r (\mathbf{v}_r^1 \otimes \mathbf{v}_r^2 \otimes \cdots \otimes \mathbf{v}_r^n), \quad (10)$$

where $\|\mathbf{v}_r\| = 1$, and for a symmetric tensor, $\mathbf{v}_r^1 = \mathbf{v}_r^2 = \cdots = \mathbf{v}_r^n$. A low-rank tensor approximation is known as rank- k decomposition and it is applied to various branches of science and engineering. It is also known in the mathematical literature as the CANDECOMP\PARAFAC (CP) decomposition [13]. The vectors \mathbf{v}_r represents here the fiber directions, and the fiber weights are simply $w_r = \lambda_r / \sum_{r=1}^k \lambda_r$. The rank of the tensor corresponds here to the number of crossing fibers within a voxel. Since we do not expect to detect reliably more than two crossing fibers using a fourth-order tensor, we restrict ourselves to the $k = 2$ case.

The fiber model is determined in this work according to the ratio between the singular eigenvalues, λ_r . That is, the weakest fiber term is rejected whenever $\lambda_{\text{strong}}/\lambda_{\text{weak}} > t$, where the threshold was set to $t = 4$. An alternative model selection approach is the core consistency diagnostic (CORCONDIA) [8]. However, it is not within the scope of this paper.

To compute the CP decomposition for a given tensor, \mathcal{D} , and a given rank, k , one has to solve the least-squares problem

$$\min_{\tilde{\mathcal{D}}} \|\mathcal{D} - \tilde{\mathcal{D}}\|^2 \quad (11)$$

where $\tilde{\mathcal{D}} = \sum_{r=1}^k \lambda_r (\mathbf{v}_r^1 \otimes \mathbf{v}_r^2 \otimes \cdots \otimes \mathbf{v}_r^n)$. Due to its simplicity and efficiency, the most popular technique to compute a rank- k tensor approximation is the Alternating Least Squares (ALS) [9, 14]. The principal of the ALS is straightforward. In each iteration it solves a least-squares problem for the set of vectors $\{\mathbf{v}_r^i\}_{r=1}^k$, $i = m$, while keeping the vectors with $i \neq m$ fixed.

A particular case with $k = 1$ is the *rank-1* decomposition. Given a symmetric tensor \mathcal{D} , its best rank-1 approximation is computed by solving the problem (11) where $\tilde{\mathcal{D}} = \lambda \underbrace{\mathbf{v} \otimes \mathbf{v} \otimes \cdots \otimes \mathbf{v}}_{n \text{ times}}$. This problem is equivalent to the nonlinear optimization problem [16]

$$\max_{\mathbf{v}} |D(\mathbf{v})| \quad \text{subject to} \quad \|\mathbf{v}\| = 1, \quad (12)$$

where $D(\mathbf{v})$ is the homogeneous polynomial induced by the tensor and identified here with the ODF. The best rank-1 decomposition for symmetric tensors can be efficiently computed by solving the ALS for $k = 1$ or by using a high-order power method (HOPM) (e.g., [15]). This problem may have multiple non-antipodal solutions and the different solutions are found by multiple initializations. Upon converges, for each initialization the algorithm produces an eigenpair $(\mathbf{v}_i, \lambda_i)$. For each eigenpair the unit-norm vector \mathbf{v}_i specifies a global maximum location where $\lambda_i = D(\mathbf{v}_i)$. As in our case $D(\mathbf{v})$ corresponds to the ODF, *as long as the*

maxima are distinguished, the resulting vectors will point in the directions of the underlying fibers. As we will show in the next section, at these cases as well, the CP decomposition is superior to maxima finding.

4 Experiments

4.1 Synthetic data simulations

To assess the accuracy of our new algorithm, we applied it to synthetic, as well as measured experimental HARDI data. First, we generated synthetic data by simulating two crossing fibers according to the multi-compartment model

$$S(\mathbf{g}, b) = S_0 \sum_{i=1}^{k=2} w_i e^{-b\mathbf{g}D_i\mathbf{g}^T}. \quad (13)$$

For both tensors we assume a prolate tensor model with eigenvalues $\lambda_1 = 1.7 \cdot 10^{-3} \text{mm}^2/\text{s}$, $\lambda_2 = \lambda_3 = 3 \cdot 10^{-4} \text{mm}^2/\text{s}$ and a b -value of 1500 s/mm^2 . The baseline signal was set to $S_0 = 1$. One fiber direction was created randomly and the second one was obtained by rotating the corresponding tensor to get the desired separation angle between the fibers. The weights were set equally. For the convolution kernel we have used Eq. (3) with a concentration parameter of $c = 200$.

The algorithm was tested on noisy data at three levels of SNR_0^1 : 50, 25 and 12.5, where the signal was corrupted by Rician distributed noise. For each noise level, the separation angle was varied from 30 to 90 in 5 degree steps. The signal was measured using 81 gradient directions which were computed using a second-order icosahedron sphere tessellation. For each separation angle and noise level, we performed 100 experiments where fourth-order tensors were estimated using the linear programming approach and a rank-2 decomposition was applied to extract the fiber directions and fractions. The mean and the standard deviation of the separation angle, the fiber direction deviation and the weights estimation were calculated for each case.

The CP decompositions were performed using the ALS algorithm [9]. Although the ALS algorithm produces non-symmetric intermediate results for symmetric tensors, we have found that eventually it converges to a symmetric tensor solution. We have implemented a symmetric version of the ALS according to [9]. Although it produces symmetric intermediate solutions, it has not obtained more accurate solutions than the non-symmetric version. For a MatLab implementation of the ALS² it takes 20ms on a Linux workstation with a 2.4MHz quad core CPU and 6GB to produce a rank-2 decomposition for a given tensor.

There are only rare cases where the ALS will not converge to a stationary point. However, it may converge to local minima. While local minima solutions cannot be entirely avoided, we have found that they can be adequately treated

¹ Measured as the baseline signal, S_0 , divided by the noise standard deviation, σ .

² Available at: <http://csmr.ca.sandia.gov/~tgkolda/TensorToolbox/>

by initializing the ALS using the singular eigenvectors of the unfolded tensor [16]. Random initialization gave less accurate results as the algorithm produced local minima solutions more often, especially in low SNR simulations and for small separation angles. The results are summarized in Fig. 1 and Fig. 2. In Fig. 1 we

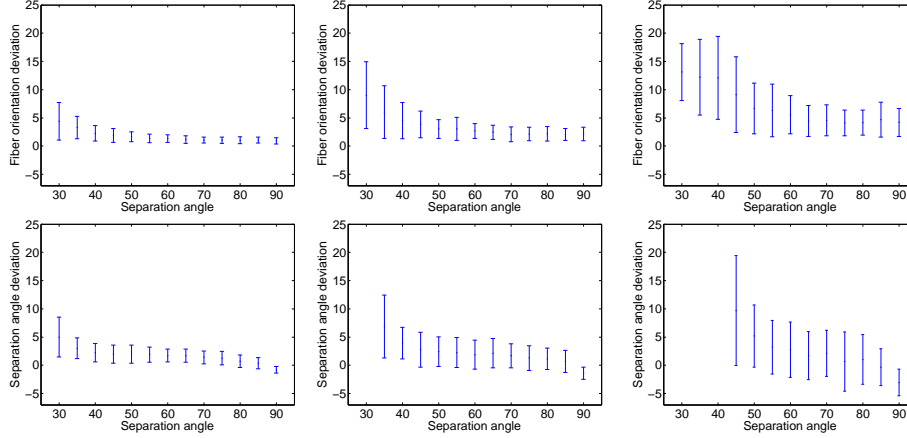


Fig. 1. The minimal fiber direction deviation (top) and separation angle deviation (bottom). The SNR decreases from left to right.

present the minimal fiber direction deviations of the estimated directions from the true directions, as well as the separation angle deviations. For SNR ratios of 50 and 25 it is shown that the algorithm can reliably resolve the fiber directions, especially above a separation angle of 35 degrees. When the SNR drops down to 12.5, which is a value found in real scans, below an angle of 45 degrees, we observed large biases and high standard deviations at one fiber direction. Hence, the separation angle deviation is not shown for these cases. The performance of the algorithm in this SNR level improves significantly above a separation angle of 50 degrees where both fiber directions could be resolved reliably. As shown in Fig. 2 the fiber fractions could be estimated accurately above 45 degrees for SNR levels of 50 and 25 whereas at the lowest SNR level 60 degrees is the point where the accuracy improves significantly. In Fig. 3 we show that the rank-2 CP decomposition has an advantage over maxima finding even at large separation angles where the ODF has distinct maxima. While at a fiber separation angle of 80 degrees the rank-2 decomposition has a slight advantage only at low SNR levels (left image), at 70 degrees it outperforms the rank-1 decomposition at all noise levels (right image). Below 70 degrees the maxima merge and maxima finding is no more reliable. In the middle image, an ODF that represents crossing fibers at 45 degrees is presented. In that case the correct fiber orientations can be estimated by using the rank-2 decomposition only. Maxima directions in this experiment were calculated using the SS-HOPM algorithm [15].

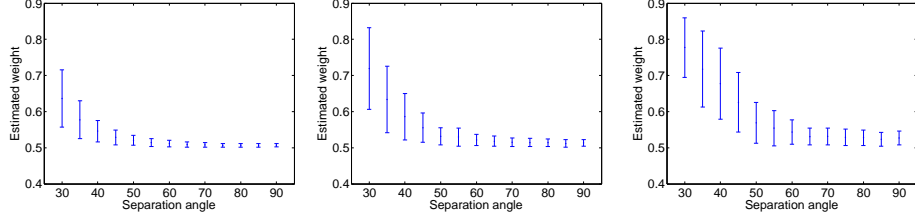


Fig. 2. The estimation of fiber fraction for one fiber using the rank-2 decomposition. The SNR ratio decreases from 50 to 12.5, from left to right.

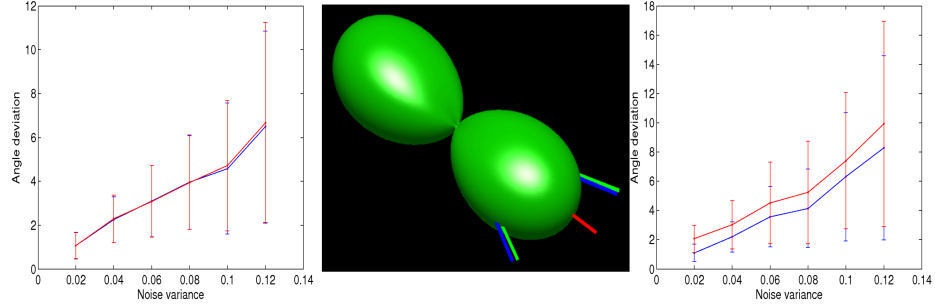


Fig. 3. Rank-2 decomposition vs. maxima finding with rank-1 decomposition. These results present the minimal fiber direction deviation for a separation angle of 80 degrees (left) and 70 degrees (right). The middle image demonstrate the differences between the approaches when the separation angle is 45 deg. The green and the blue lines show the true and the estimated fiber directions, respectively. The red line shows the direction of the maximum obtained by a rank-1 tensor decomposition. The mean and the standard deviation were calculated from 100 experiments for each noise level.

4.2 Phantom data

To test our algorithm on experimentally obtained HARDI data where the ground truth fibers are known, we first apply our decomposition algorithm to the publicly available phantom data used in the MICCAI 2009 Fiber Cup contest [18]. The data was scanned at three b-values: 650, 1500 and 2650 s/mm². We used the dataset with a b-value of 2650s/mm² in this study. The top row of Fig. 4 shows the reconstructed fourth-order tensor field, the rank-1 decomposition and the rank-2 decomposition results. The two right hand side images in this row illustrate the comparison between the rank-1 and the rank-2 decomposition where the differences between the decompositions are highlighted by ellipses. The fiber directions are presented as thin cylinders at each voxel, where the length of the cylinder is determined by the fiber weight. We have integrated the ground truth fibers as a reference.

As shown, the decomposed directions clearly delineate the hidden fiber orientations. However, by using the rank-2 decomposition, our algorithm could detect more crossing fibers which are oriented along the ground truth fibers.

4.3 Cat brain data

To test the algorithm on real data we used a HARDI scan of a cat brain. The data was acquired using a standard 3D diffusion-weighted spin-echo sequence with $TR=500$ ms, $TE=39.8$ ms, field of view $70 \times 40 \times 32$ mm, matrix size $175 \times 100 \times 80$, zero padded to $200 \times 100 \times 80$, yielding an isotropic resolution of 400 microns and a b-value of 6000 s/mm². Four images without diffusion weighting (b0 image) and 96 diffusion weighted images were acquired. The diffusion gradients were uniformly spaced over a unit sphere. The two left images of the bottom row in Fig. 4 show the b0 image and the reconstructed fourth-order tensor field for the two specified ROIs. The two right images in this row compare between maxima finding with the rank-1 decomposition and the rank-2 decomposition. These results show that some of the crossing fibers, which are not detectable using maxima finding, could be detected using the rank-2 decomposition. Although further validation needs to be done on more datasets, promising results are already demonstrated qualitatively on this cat brain data.

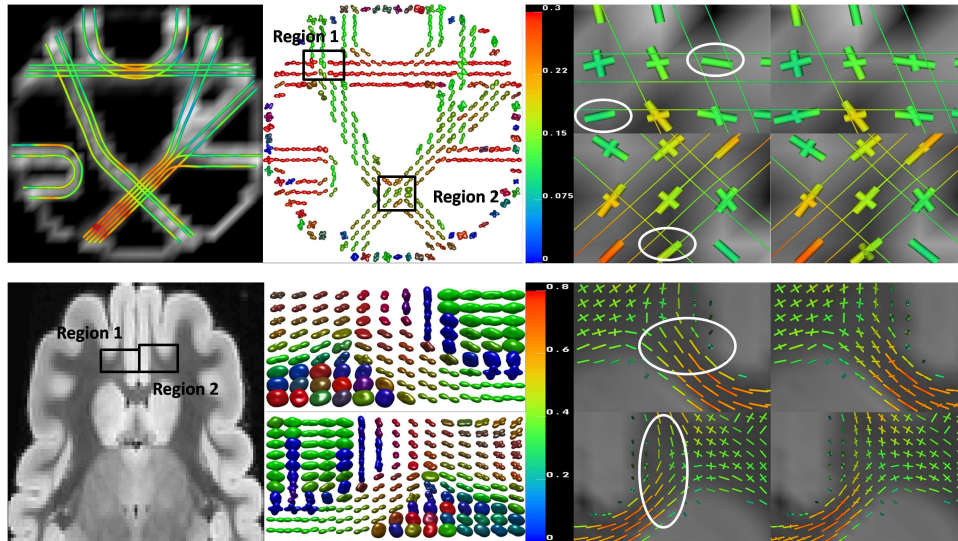


Fig. 4. The decomposition results of the ODF field of the phantom (top row) and cat brain (bottom row) show the following: b0 image (left), fourth-order tensor field of region 1 and region 2 (middle left), rank-1 decomposition (right middle) and rank-2 decomposition (right). The results of region 1 are presented at the top and the results of region 2 are at the bottom. For the phantom, the ground truth fibers are shown both in the b0 image and in the detailed views of the decomposition results.

5 Conclusions

In this paper we propose a novel framework that combines an ODF estimation method with a parameter extraction technique for estimation of fiber directions and fiber fractions. For the estimation method we have used a specific form of spherical deconvolution where the ODF is represented by a homogeneous polynomial induced by a high-order tensor. The ODF was constrained to be non-negative by adding a set of linear constraints to the objective function that represents the spherical deconvolution. Then, we show that fiber directions and fiber fractions are accurately extracted by applying a rank-2 CP decomposition to the ODF. As the ODF in this case is associated with a high-order tensor we can apply the decomposition directly to the tensor without using the conversion step which was necessary in [19]. The CP decomposition optimizes the *sum* of the different rank-1 terms and no tensor subtractions are being used. Consequently, the problems of rank increasing and non-positive residuals do not exist here.

Experiments were performed on synthetic data, phantom and real data show that this method can resolve two crossing fibers reliably, even at low SNR, and at far better resolution than the maxima detection approach.

As future work we plan to make the algorithm more efficient, accurate and more robust to noise both at the spherical deconvolution and the tensor decomposition levels. Tensors of order greater than four will be considered as well.

Acknowledgments

The authors would like to thank Tamara G. Kolda of Sandia National Labs, Livermore, California, for useful discussions and comments regarding this work. This research was funded by the NIH grants: 5R01EB007688, 5R01HL092055, and by the NIH/NCRR Center for Integrative Biomedical Computing, P41-RR12553-10, Award No. KUS-C1-016-04, made by King Abdullah University of Science and Technology (KAUST), and DOE SciDAC VACET.

References

1. Iman Aganj, Christophe Lenglet, and Guillermo Sapiro. ODF maxima extraction in spherical harmonic representation via analytical search space reduction. In *MICCAI'10*, volume 6362 of *LNCS*, pages 84–91. 2010.
2. Daniel C. Alexander. Maximum entropy spherical deconvolution for diffusion MRI. In *IPMI'05*, volume 3565 of *LNCS*, pages 76–87, 2005.
3. Kendall Atkinson. Numerical integration on the sphere. *J. Austral. Math. Soc.*, 23:332–347, 1982.
4. Angelos Barmpoutis, M. S. Hwang, D. Howland, J. R. Forder, and Baba C. Vemuri. Regularized positive-definite fourth-order tensor field estimation from DW-MRI. *NeuroImage*, 45(1):153–162, 2009.
5. Angelos Barmpoutis, Bing Jian, and Baba C. Vemuri. Adaptive kernels for multi-fiber reconstruction. In *IPMI'09*, volume 5636 of *LNCS*, pages 338–349, 2009.

6. Angelos Barmpoutis and Baba C. Vemuri. A unified framework for estimating diffusion tensors of any order with symmetric positive-definite constraints. In *ISBI'10*, pages 1385–1388, 2010.
7. Luke Bloy and Ragini Verma. On computing the underlying fiber directions from the diffusion orientation distribution function. In *MICCAI'08*, volume 5241 of *LNCS*, pages 1–8, 2008.
8. Rasmus Bro and Henk A. L. Kiers. A new efficient method for determining the number of components in parafac models. *J. of Chemometrics*, 17:274–286, 2003.
9. P. Comon, X. Luciani, and A. L. F. de Almeida. Tensor decompositions, alternating least squares and other tales. *J. of Chemometrics*, 23:393–405, 2009.
10. M. Descoteaux; E. Angelino; S. Fitzgibbons; R. Deriche. Regularized, fast, and robust analytical Q-ball imaging. *Magn. Res. Med.*, 58(3):497–510, 2007.
11. M. Grant and S. Boyd. CVX: Matlab software for disciplined convex programming, version 1.21. <http://cvxr.com/cvx>, October 2010.
12. Johan Håstad. Tensor rank is NP-complete. *J. Algorithms*, 11:644–654, 1990.
13. H. A. L. Kiers. Towards a standardized notation and terminology in multiway analysis. *J. of Chemometrics*, 14:105–122, 2000.
14. Tamara G. Kolda and Brett W. Bader. Tensor decompositions and applications. *SIAM Review*, 51:455–500, 2009.
15. Tamara G. Kolda and Jackson R. Mayo. Shifted power method for computing tensor eigenpairs. arXiv:1007.1267v2 [math.NA], Feb 2011.
16. L. De Lathauwer, B. De Moor, , and J. Vandewalle. On the best rank-1 and rank- (r_1, r_2, \dots, r_n) approximation of higher-order tensors. *SIAM Journal on Matrix Analysis and Applications*, 21:1324–1342, 2000.
17. Evren Özarslan, Timothy M. Shepherd, Baba C. Vemuri, Stephen J. Blackband, and Thomas H. Mareci. Resolution of complex tissue microarchitecture using the diffusion orientation transform (DOT). *NeuroImage*, 31(3):1086–1103, 2006.
18. C. Poupon, B. Rieul, I. Kezele, M. Perrin, F. Poupon F, and JF. Mangin. New diffusion phantoms dedicated to the study and validation of high-angular-resolution diffusion imaging HARDI models. *Magn Reson Med*, 60(6):1276–1283, 2008.
19. Thomas Schultz and Hans-Peter Seidel. Estimating crossing fibers: A tensor decomposition approach. *IEEE Transactions on Visualization and Computer Graphics (Proc. IEEE Visualization)*, 14(6):1635–1642, 2008.
20. Thomas Schultz, Carl-Fredrik Westin, and Gordon Kindlmann. Multi-diffusion-tensor fitting via spherical deconvolution: A unifying framework. In *MICCAI'10*, volume 6361 of *LNCS*, pages 673–680, 2010.
21. Alwin Stegeman and Pierre Comon. Subtracting a best rank-1 approximation may increase tensor rank. *Linear Algebra and its Applications*, 433:1276–1300, 2010.
22. J.-Donald Tournier, Fernando Calamante, David G. Gadian, and Alan Connelly. Direct estimation of the fiber orientation density function from diffusion-weighted MRI data using spherical deconvolution. *NeuroImage*, 23(3):1176 – 1185, 2004.
23. Antonio Tristan-Vega, C.-F. Westin, and Santiago Aja-Fernandez. Estimation of fiber orientation probability density functions in high angular resolution diffusion imaging. *NeuroImage*, 47(2):638–650, 2009.
24. David S. Tuch. Q-ball imaging. *Magn. Res. Med.*, 52(6):1358–1372, 2004.
25. David S. Tuch, Timothy G. Reese, Mette R. Wiegell, Nikos Makris, John W. Belliveau, and Van J. Wedeen. High angular resolution diffusion imaging reveals intravoxel white matter fiber heterogeneity. *Magn. Res. Med.*, 48(4):577–582, 2002.
26. Yonas Weldeselassie, Angelos Barmpoutis, and M. Atkins. Symmetric positive-definite cartesian tensor orientation distribution functions (CT-ODF). In *MICCAI'10*, volume 6361 of *LNCS*, pages 582–589, 2010.